

Transport in Molecular Junctions with Different Metallic Contacts

John W. Lawson* and Charles W. Bauschlicher, Jr.†

Mail Stop 269-2

Center for Nanotechnology

NASA Ames Research Center

Moffett Field, CA 94035

Abstract

Ab initio calculations of phenyl dithiol connected to Au, Ag, Pd, and Pt electrodes are performed using non-equilibrium Green's functions and density functional theory. For each metal, the properties of the molecular junction are considered both in equilibrium and under bias. In particular, we consider in detail charge transfer, changes in the electrostatic potential, and their subsequent effects on the IV curves through the junctions. Gold is typically used in molecular junctions because it forms strong chemical bonds with sulfur. We find however that Pt and Pd make better electrical contacts than Au. The zero-bias conductance is found to be greatest for Pt, followed by Pd, Au, and then Ag.

*Electronic address: John.W.Lawson@nasa.gov

†Electronic address: Charles.W.Bauschlicher@nasa.gov

I. INTRODUCTION

Interest in electrical conduction in molecules has been spurred in recent years by many experimental results where transport in individual molecules was measured. A number of interesting and potentially technologically useful phenomena have been catalogued from switching [1], nondifferential resistance [2], and transistor action [3] to more exotic behavior such as Kondo physics [4] and vibronic effects [5]. In parallel with these developments has been theoretical work, ranging from semi-empirical theories [6] to ab initio formalisms based on non-equilibrium Green's functions (NEGF) and density functional theory (DFT) [7, 8, 9, 10, 11, 12, 13, 14, 15, 16]. Many open questions remain including the large discrepancy between theoretical and experimental current-voltage IV curves as well as attempts to obtain more accurate experimental characterization of the junctions.

Phenyl dithiol (PDT) attached to Au electrodes has become an important prototypical system. This is due in part to important early experiments[17], but is also due to its accessibility to a number of high-powered theoretical tools. Experimental interest in Au contacts is largely one of convenience, since Au is known to make good chemical contact with the thiol end groups. Whether this results in an optimal electrical contact is less clear. It is important therefore to examine the conduction properties of PDT connected to other metals in an effort to find the combination with optimal performance characteristics.

In this paper, we compare in detail the transport properties of PDT with Ag, Au, Pd, and Pt contacts. Experimental investigations of molecular junctions with electrodes other than gold have included molecular hydrogen attached to Pd and Pt [18] as well as more complicated organic molecules in contact with different metals [19]. To our knowledge, there has not been an experimental study of PDT with non-gold contacts. Early theoretical analysis of these systems has appeared [20]. However, a simpler formulation was utilized than what we use, especially with respect to the description of the contacts, which is our main object of study. Our results show significant differences from that previous work. Yaliraki et al [21] using a non-self-consistent method considered Ag in addition to Au. They found Ag to be a worse conductor than Au consistent with our results. Di Ventura et al. [22] considered Al contacts in addition to Au, finding the Al junction to have better conduction characteristics. In addition to current-voltage (IV) characteristics, we consider the role of charge transfer and changes in electrostatic potential due to formation of the contacts, both

at equilibrium and under bias.

In general, the tunneling current through a molecular junction depends on the electronic structure of the junction in the vicinity of the Fermi level. We found that junctions with different metal electrodes result in qualitatively different conduction characteristics. We employed a first principles method based on NEGF and DFT. This allowed us to consider the interplay of issues related to charge transfer and band lineup due to the formation of contacts under equilibrium condition as well as nonequilibrium transport through the junction under bias.

II. METHOD

We utilized the methodology developed by Xue, Datta, and Ratner [23]. The NEGF code has been interfaced with Gaussian03, which allows us access to the full suite of basis sets and functionals offered by Gaussian03 to describe our systems. Details of our calculational approach and methodology have been reported elsewhere [23, 24, 25, 26, 27, 28]. We recall the most salient features briefly for completeness.

Clusters of atoms from each metal contact are added to the ends of the molecule to form an “extended molecule”. The extended molecule is then further connected to additional atoms in the electrodes. This coupling is implemented through a Green’s function approach

$$G(E) = 1/(ES - F - \Sigma_L(E) - \Sigma_R(E)) \quad (1)$$

where F is the Fock matrix of the extended molecule, S is the overlap matrix, and $\Sigma_L(E), \Sigma_R(E)$ are self-energies that define the couplings to the contacts. The self-energies are defined as

$$\Sigma(E) = \tau^T g_s(E) \tau \quad (2)$$

where τ is a matrix that gives the couplings between the extended molecule and atoms in the contacts and $g_s(E)$ is a matrix representing the surface Green’s function for a semi-infinite bulk metal. The density of states (DOS) for the metal surfaces can be recovered by $DOS(E) = -Im(g_s(E))/2\pi$.

From the Green’s function, the density matrix is calculated as

$$\rho = \frac{1}{2\pi i} \int_C dE G(E) \quad (3)$$

and, thus within a DFT framework, a self-consistent field (SCF) procedure can be devised. Self-consistent methods are necessary to describe charge transfer effects correctly. Since $G(E)$ has a non-trivial energy dependence through $\Sigma(E)$, the integral is performed using a numerical complex contour technique.

Once a self-consistent Green's function has been obtained, the transmission function can be evaluated using the Landauer relation

$$T(E) = \text{Tr}[\Gamma_L(E)G(E)\Gamma_R(E)G^\dagger(E)]. \quad (4)$$

where $\Gamma(E) = i(\Sigma(E) - \Sigma(E)^\dagger)$ is the coupling function that gives information about the quality of the contact between the molecule and the electrodes as well as information about the density of states in the bulk available for current transmission across the junction. The transmitted current can be calculated at zero temperature as the integral of the transmission function

$$I = \frac{2e}{h} \int_{E_f-V/2}^{E_f+V/2} T(E)dE \quad (5)$$

in a energy window of width V around the Fermi energy E_f . Generalizing this result to finite temperature is straightforward.

The self-energy $\Sigma(E)$ contains not only geometric and electronic information about the contacts, but also defines the strength of the coupling between the molecule and the electrode. The self-energy also acts as an energy dependent, complex-valued potential. Its effect in modeling the contacts is to shift and broaden the energy levels of the molecule, determine the density of states available to be transmitted from the metal, and give the strength of the coupling to the molecule. All of these factors affect the transmission spectra of the junction. A comprehensive discussion of the NEGF approach to transmission is given by Datta [29].

Evaluation of $\Sigma(E)$ is made tractable by the fact that elements of τ are nonzero for only a distance of several atomic layers from the extended molecule. In this work, the τ matrices are constructed from tight binding (TB) parameters [30] where nine orbitals per Au atom have been used. The TB parameters were obtained from fits to first principles band structure calculations. The surface Green's function $g_s(E)$ for the semi-infinite metals is constructed using a recursive procedure [31]. The Green's function is decomposed into a sum

$$g_s(\vec{R}, E) = \sum_{\vec{k}} g_{\vec{k}}^0(y, E) e^{i\vec{k}\cdot\vec{r}} \quad (6)$$

where g_k^0 are Fourier components in the first principal layer parallel to the surface and \vec{r} and \vec{k} are vectors parallel to the surface. Each g_k^0 is coupled successively to components g_k^n residing in the n^{th} principal layer deeper in the bulk. This process is continued until the surface components g_k^0 converge. For computational expediency, tight binding parameters are used to build the coupling matrices to start the iteration. This is the principle approximation for constructing $\Sigma(E)$. There are no free parameters in this formalism.

III. MODEL

A potential difficulty of our approach is the fact that the extended molecule is described with DFT while the self-energies $\Sigma(E)$, which represent the wider electrodes, are constructed using tight binding parameters. This mismatch of microscopic descriptions may affect the quality of the contact, and lead, for example, to spurious reflections at the boundary of the two regions. To test this possibility, we examined transmission through linear atomic chains where the chains and electrodes were composed of the same metallic elements. In these cases, we expect an especially good contact to result and also expect the transmission to approximate the theoretical maximum given by the quantum of conductance.

In particular, we considered linear chains of six metallic atoms for Au, Pt, Pd, and Ag. The geometries considered are shown in Fig. 1. Atoms in the first surface layer are added explicitly to the extended molecule and are then included in the self-consistent field calculations. Additional atoms in the both the first and second layers also coupled to the extended molecule through the self-energies, although their orbitals remain fixed during the SCF. The Fermi energies used were $E_f = -5.31\text{eV}$ for Au, $E_f = -5.6\text{eV}$ for Pd, $E_f = -5.93\text{eV}$ for Pt, and $E_f = -4.74\text{eV}$ for Ag. The interatomic spacings within the chains were optimized and bulk positions were used for the clusters attached at each end. Equilibrium transmission spectra and IV characteristics were calculated for the different metals with clusters of 6, 12, and 21 atoms included on each side on the extended molecule. In Fig. 2, we show results for gold which are representative. The main graph is the transmission spectra while the inset is the IV curves from zero to one volt. In the IV curve, the upper dotted line gives the theoretical maximum. Clearly, as the size of the cluster increases, there is a significant increase in the transmission especially near the Fermi level. The results for the 21 atom cluster are very close to the quantum of conductance. There is a small

overestimation of the transmission near the Fermi level. This is an artifact of the TB approximation of $\Sigma(E)$. Based on these results, we used the larger clusters in subsequent calculations.

The junctions we considered consist of a single molecular fragment, PDT, $-S-C_6H_4-S-$ bonded to two parallel, semi-finite metallic electrodes. It should be noted that this is a non-periodic calculation. Therefore, we model a single molecule, rather than an array. The electrodes are represented by clusters of 21 atoms taken from the first surface layer and included into the extended molecule and therefore into the self-consistent field calculation. An additional 63 atoms from both the first and second layers are coupled to the extended molecule through $\Sigma(E)$. However, the orbitals for these atoms do not relax self-consistently, but are fixed to their TB values. The geometry of the extended molecule used is shown in Fig. 3. The axis of the molecule is parallel to the cartesian y -axis while the Au surfaces run parallel to the xz -plane. The geometry of PDT was optimized with H atoms attached to the S, and for each metal we optimized the metal-S bond length after removing the terminal H atoms. It is important to note that to determine the bond lengths, we optimized the energy of the entire junction including the effects of the self-energies. We found significant variation using simpler models, differing basis sets, or by neglecting the self-energies. The results were $d = 2.379\text{\AA}$ for gold, $d = 2.569\text{\AA}$ for platinum, $d = 2.776\text{\AA}$ for palladium, and $d = 2.876\text{\AA}$ Silver. The sulfur were positioned over the hollow of the $\langle 111 \rangle$ surface and the molecule was oriented at 90 degrees to the surface. This orientation has been shown in previous work [32], and by others, to be the low energy configuration.

The electronic cores of the molecule (C,S) were replace by compact effective potentials (CEP). The valence electrons were described by the CEP-121G basis set where we have added polarization functions to the carbon and hydrogen and diffuse and polarization functions to the sulfur. Previous work has shown [28] that inclusion of polarization/diffuse functions has an important impact on the results. In particular, larger currents were observed for the basis set CEP121+G* as the sulfur was able to make a better contact with the electrodes [28].

For the metallic atoms, we utilize the LANL1 pseudopotential and a “reduced/optimized” minimal basis set. For Au and Pt, this means removing the most diffuse s,p, and d Gaussian primitives from basis functions, and for Pd and Ag, removing only the most diffuse s and p. Previous work [24, 33] as shown that elimination of the most diffuse functions on the metal

atoms reduces unphysical super-charging of the contacts and also improves convergence. Any residual charging can be further reduced to zero by optimizing the the d-electron basis set (in particular, the most diffuse d functions) and also by adding a small field ($5\text{-}10\text{E-}4$ a.u.) to the contacts. This has the effect analogous to periodic calculations where the Hartree potential is forced to maintain the bulk values deep inside the electrodes.

All electronic structure calculations were performed at the DFT level using Gaussian03. Green's function calculations were performed using the code described previously. We mainly used the hybrid functional B3PW91 [35, 36] due to its greater accuracy, although we also used other functionals, such as BPW91, for purposes of comparison. Previous work has shown that hybrid functionals tend to reduce the magnitude of the current reflecting the effects of exchange [28]. All calculations are done at zero temperature.

IV. RESULTS AND DISCUSSION

We began by considering the zero bias equilibrium situation to examine the effects of the binding of the molecule to the metallic electrodes. To compare the degree of charge transfer for the different electrodes, we considered the spatial distribution of the charge redistribution resulting from the junction formation. As an example, we show in Fig. 4 the spatial profile of charge redistribution for the Ag junction that has the largest transfer. The figure is an XY plot, where the results have been averaged in the z -direction, of the difference between the charge density of the device at equilibrium and the contact plus the bare molecule densities taken alone. We see that the binding of the sulfur to the metallic Ag atoms results in charge transfer to the sulfur and the adjacent carbon. We further note a depletion of charge in the region between the S-C atoms which indicates a weakening of those bonds.

For all four metals, we see a similar pattern, but with different magnitudes. In Fig. 5, we further averaged over the x -direction to compare charge transfer along the axis of the molecule between the different junctions. We indicate the y -coordinate of the molecular atoms on the horizontal axis. We see that Ag has the largest charge transfer following by Au, Pt, and then Pd.

To gain further insight into junction formation, we also examine the corresponding change in the electrostatic potential energy. In Fig. 6, we show the full spatial profile for Ag, the metal with the largest redistribution. For the potential profile, we show a cross-section

of the potential taken in the XY plane ($z = 0$). The z-direction has not been averaged in order to display the potential energy the electron actually sees. Potential barriers are formed on the sulfur atoms as well as on the interior carbons. These barriers are relevant for tunneling electrons through the junction under bias. In Fig. 7, we compare the potential energy redistributions along the axis of the molecule. We see that Ag has the largest barriers to overcome for electron transport and Pt the smallest. On this basis, we might guess that Pt would make the best conductor and Ag the worst. We also note that Ag has a barrier twice that of Au and four times that of Pt.

The self-consistent change in potential affects the electronic structure of the molecule, leading to a lineup of molecular states with the continuum of states residing in the electrodes. In order for there to be transmission, there must be finite density of states in the contacts to be transmitted. The surface DOS can be calculated from the surface Green's function $g_s(E)$ as $DOS(E) = -Im(g_s(E))/2\pi$. We compare the DOS for the metals in Fig. 8. The energy scale is given relative to the individual Fermi energies. We see from the figure that in all cases there are states available at the Fermi level for transport. We notice in particular that while for Au and Ag, the DOS is rather flat, for Pt and Pd, the DOSs are rapidly increasing near their Fermi energy.

The self-consistent change in potential affects the electronic structure of the molecule, leading to a lineup of molecular states with the continuum of states residing in the electrodes. The affect of this lineup as well as the level broadening due to coupling the contacts can be seen directly in the transmission spectrum $T(E)$. The transmission spectra of the molecule with the different metals are displayed in Fig. 9. One of the most visible features of the spectra are the large gap starting near the Fermi energy and continuing up to 4-5 eV. This corresponds to the HOMO-LUMO gap. In addition, the spectra are composed of a series of peaks whose centers correspond to a conducting state of the junction and whose width and height reflects how strongly that state is coupled to the contacts. For low voltages, it is the peaks closest to the Fermi energy that will dominate the transport. We see in the four cases that we considered that the Fermi energy lies closest to the HOMO. Therefore, it is the characteristics of the HOMO that will determine many of the features of conduction in these junctions. Furthermore, we can read off the zero bias conductance which is given by $G = T(E_f)$ in units of $2e/h$. For our junctions, Pt has the highest conductance with $G = 0.99$. After that, we obtain $G = 0.29$ for Pd, $G = 0.29$ for Au and $G = 0.11$ for Ag.

The spatial character of the channels appearing in the transmission spectrum can be examined with the local density of states (LDOS). The LDOS can be extracted directly from the Green’s function,

$$\rho(\vec{r}, E) = -ImTr(G(\vec{r}, E)). \quad (7)$$

where the trace is taken over the orbital indices. Understanding the spatial profile of conduction channels is important for engineering molecular devices. If we want to affect a particular channel, the LDOS will tell us where to focus our efforts. For example, if a channel is localized on a sulfur, then we may want to substitute a different atom at that site to get a desired behavior.

In general, we find conducting states of two basic types. The first are states based on the molecular bridge. Typically, these states are extended, conjugated, π -bonding states, that span the molecule and are expected to make good channels to transport electrons. The other type of state results from the strong hybridization of the molecule with metallic states of the contacts.

In Fig. 10, we compare the LDOS for the HOMO and LUMO transmission channels for the four junctions. As in previous plots, we have averaged over the x and z directions and show the spatial profile along the axis of the molecule. In all cases, the HOMOs appear to have strong weight on the sulfur while the LUMOs are more distributed across the molecule. This is important since it is the HOMO which controls the low bias transport.

The low bias current can be inferred from the equilibrium transmission spectrum or calculated directly. In Fig. 11, we show the full IV characteristics for the different junctions. Self-consistent calculations were performed for each bias value. Notice that flat sections of the IV curve correspond to gaps in the transmission whereas steep areas signal a new peak entering the integration window. For the Au IV curve, there is a small dip in the current for bias of 1 – 1.5V. We do not believe this is non-differential resistance (NDR). In previous work [37], we have seen such bumps, but found improving the basis set made them disappear.

A comparison of our IV curves with those of Seminario et al. [20] shows some significant differences. First, they have a much larger variation in current flow with metal. For example at a bias of 1V, Pd appears to carry at least two orders of magnitude more current than Au, while we find very similar currents for Pd and Au. They also find that Pd has the largest current flow up to biases of 5V, while we find Pt has the largest current flow.

The formalism used by Seminario et al. [38], while in the spirit of many early calculations, is significantly different from ours especially with respect to the calculation of the self-energy $\Sigma(E)$. We believe this explains the difference between our results. In their formulation, the surface Green’s function g_s that appears in Σ is a constant, diagonal matrix whose elements are the values of the partial densities of states at E_f . No other electronic structure information is included in g_s . Σ , therefore, does not depend on energy, and there is no contour integration in their calculations. There is no recursive method to model the structure of the semi-infinite bulk contacts. They use a “fitting” parameter to fix the coupling. Furthermore, the metal clusters are much smaller than what we use, typically 1-5 Au atoms.

We can also consider charge density redistribution inside the junction under bias. It has been pointed out that resistivity dipoles can form due to charge buildup in the junction [24, 39]. We find similar effects in the four junctions we considered. As an example in Fig. 12, we show the spatial profile of the charge density redistribution for Pd at a bias of 1.8V. The difference relative to the equilibrium density is shown. We see a large spike on the left-most carbon and sulfur. For comparison, we plot in Fig. 13 the density profiles along the y-axis for all the junctions. Interesting, we see that the largest charge buildup within a junction does not occur at the same place for the different metals. For Pd and Pt, the charge buildup occurs on both sides of C and S, while for Au and Ag, it occurs on the right. The inset gives the density redistribution relative to the isolated molecule and contacts. This figure should be compared with Fig. 5 to show how the charge buildup affects the original equilibrium charge transfer. In particular, we see a reduction on the right of charge accumulation and an enhancement on the left. This will affect the respective barrier heights.

Furthermore, we can examine the corresponding change in electrostatic potential. Again, for Pd, we show in Fig. 14, the spatial cross section in the XY plane of the difference between the bias induced potential and equilibrium. In Fig. 15, we compare the potential profiles for the different junctions. Interesting, there is a spread in the curves for the different metals inside the junction despite the fact that all the junctions have the same molecule. These are effects imposed by the contacts and reflect the differing polarization inside the molecule as shown in Fig. 13.

V. CONCLUSION

We have performed detailed ab initio calculations of the conduction properties of PDT connected to Au, Pd, Pt, and Ag electrodes. We were able to consider the interplay between equilibrium effects like charge transfer, electrostatics, and band lineup in the formation of the junction. The transmission spectra and the LDOS allowed us to identify the dominant channels for conduction. In particular, we could consider the spatial distribution of the HOMO and LUMO and identify where in the molecule these states had greatest weight.

Furthermore, we found that charge transfer in the case of Au and Ag was larger than with Pd and Pt, resulting in correspondingly larger barriers. This is directly reflected in the transport properties where Pt followed by Pd had the greatest conductance. Au and Ag on the other hand had the worst. We were also able to consider in detail the effect of the external bias on the redistribution of the charge density and the electrostatic potential. In particular, we could see a reduction in the magnitude of the charge buildup resulting from the formation of resistivity dipoles inside the junctions. Interesting, the location and magnitude of the dipoles varied by junction.

VI. ACKNOWLEDGMENTS

C.W.B. is a civil servant in the Space Technology Division (Mail Stop 230-3), while J.W.L. is a civil servant in the TI Division (Mail Stop 269-2).

-
- [1] J. Chen, M.A. Reed, A.M. Rawlett and J.M. Tour, *Science*, 278 (1997) 252
 - [2] N.P. Guisinger, M.E. Greene. R. Basu, A.S. Baluch and M.C. Hersam *Nano Lett* 4 (2004) 55
 - [3] P. Avouris, P.G. Collins and M.S. Arnold, *Science* 292 (2001) 706
 - [4] J. Park, A.N. Pasupathy, J.I. Coldsmith, C. Chung, Y. Yaish, J.R. Petta, M. Rinkoski, J.P. Sethna, H.D. Abruna, P.L. McEuen, and D.C. Ralph, *Nature*, 417 (2002)
 - [5] W. Ho, X.H. Qiu, and G.V. Nazin, *Phys. Rev. Lett.* 92 (2004) 206102
 - [6] F. Zahid, M. Paulsson, E. Polizzi, A. Ghosh, L. Siddiqui and S. Datta, *J. Chem. Phys.* 123 (2005) 064707
 - [7] Y. Xue, S. Datta, M.A. Ratner, *J. Chem. Phys.* 115 (2001) 4292

- [8] P.A. Derosa, J.M. Seminario, J. Phys. Chem. B 105 (2001) 471
- [9] E.G. Emberly, G. Kirczenow, Phys. Rev. B 64 (2001) 235412
- [10] P. Damle, A.W. Ghosh, S. Datta, Chem. Phys. 281 (2002) 171
- [11] M. Di Ventura, S.T. Pantelides, N.D. Lang, Phys. Rev. Lett. 84 (2000) 979
- [12] L.E. Hall, J.R. Reimers, N.S. Hush, and K. Silverbrook, J. Chem. Phys. 112 (2000) 1510
- [13] J. Taylor, H. Guo, J. Wang, Phys. Rev. B 63 (2001) 245407.
- [14] J. Taylor, M. Brandbyge, K. Stokbro, Phys. Rev. B 68 (2003) 121101
- [15] H. Ness, S. A. Shevlin, A. J. Fisher, Phys. Rev. B 63 (2001) 125422
- [16] M. Magoga, C. Joachim, Phys. Rev. B 56 (1997) 4722
- [17] M.A Reed, C. Zhou, C.J. Miller, T.P. Burgin and J.M. Tour, Science 278 (1997) 252
- [18] R.H.M Smit, Y. Noat, C. Untiedt, N.D. Lang, M.C. van Hemert and J.M. van Ruitenbeek, Nature 419 (2002) 906; S. Csonka, A. Halbritter, G. Mihaly, O.I. Shklyarevshii, S. Speller and H. van Kempen, Phys. Rev. Lett. 93 (2004) 016802
- [19] D. Bong, I. Tam and R. Breslow, JACS 126 (2004) 11796; L.T. Cai, H. Shulason, J.G. Kushmerick, S.K. Pollack, J. Naciri, R. Shashidhar, D.L. Allara, T.E. Mallouk, and T.S. Mayer, J. Phys Chem. B 108 (2004) 2827
- [20] J.M. Seminario, C.E. De La Cruz, and P.A. Derosa, JACS 123 (2001) 5616
- [21] S.N. Yaliraki, M. Kemp, and M. Ratner, JACS, 121, (1999), 3428
- [22] M. Di Ventura, N.D. Lang, S.T. Pantelides, Chem. Phys, 281, (2002), 189
- [23] Y. Xue, S. Datta, M.A. Ratner, Chem. Phys. 281 (2002) 151
- [24] Y. Xue, M.A. Ratner, Phys. Rev. B 68 (2003) 115406
- [25] Y. Xue, M.A. Ratner, Phys. Rev. B 68 (2003) 115407
- [26] Y. Xue, M.A. Ratner, Phys. Rev. B 69 (2004) 085403
- [27] Y. Xue, Ph.D. thesis, School of Electrical and Computer Engineering, Purdue University (2000).
- [28] C. W. Bauschlicher, J. W. Lawson, A. Ricca, Y. Xue and M. A. Ratner, Chem. Phys. Lett. 388 (2004) 427
- [29] S. Datta, *Electron Transport in Mesoscopic Systems*, Cambridge, 1995
- [30] D.A. Papaconstantopoulos, *Handbook of the Band Structure of Elemental Solids* (Plenum Press, New York, 1986)
- [31] F. Guinea, C. Tejedor, F. Flores, and E. Louis, Phys. Rev. B 28 (1983) 4397

- [32] C.W. Bauschlicher and A. Ricca, Chem. Phys. Lett. 367, (2003) 90
- [33] C.W. Bauschlicher and Y. Xue, Chem. Phys. 315 (2005) 293
- [34] Gaussian 03, Revision B.05, M. J. Frisch, G. W. Trucks, H. B. Schlegel, G. E. Scuseria, M. A. Robb, J. R. Cheeseman, J. A. Montgomery, Jr., T. Vreven, K. N. Kudin, J. C. Burant, J. M. Millam, S. S. Iyengar, J. Tomasi, V. Barone, B. Mennucci, M. Cossi, G. Scalmani, N. Rega, G. A. Petersson, H. Nakatsuji, M. Hada, M. Ehara, K. Toyota, R. Fukuda, J. Hasegawa, M. Ishida, T. Nakajima, Y. Honda, O. Kitao, H. Nakai, M. Klene, X. Li, J. E. Knox, H. P. Hratchian, J. B. Cross, C. Adamo, J. Jaramillo, R. Gomperts, R. E. Stratmann, O. Yazyev, A. J. Austin, R. Cammi, C. Pomelli, J. W. Ochterski, P. Y. Ayala, K. Morokuma, G. A. Voth, P. Salvador, J. J. Dannenberg, V. G. Zakrzewski, S. Dapprich, A. D. Daniels, M. C. Strain, O. Farkas, D. K. Malick, A. D. Rabuck, K. Raghavachari, J. B. Foresman, J. V. Ortiz, Q. Cui, A. G. Baboul, S. Clifford, J. Cioslowski, B. B. Stefanov, G. Liu, A. Liashenko, P. Piskorz, I. Komaromi, R. L. Martin, D. J. Fox, T. Keith, M. A. Al-Laham, C. Y. Peng, A. Nanayakkara, M. Challacombe, P. M. W. Gill, B. Johnson, W. Chen, M. W. Wong, C. Gonzalez, and J. A. Pople, Gaussian, Inc., Pittsburgh PA, 2003.
- [35] A.D. Becke Phys Rev A 38 (1988) 3098
- [36] J.P. Perdew, Y. Wang, Phys Rev B 45 (1991) 13244 Cambridge, 1995)
- [37] C. W. Bauschlicher, J. W. Lawson, Chem. Phys., 324, (2006), 647
- [38] P. Derosa and J. Seminario, J.Phys.Chem. B, 105, (2001) p471
- [39] R. Landauer, IBM J. Res. Dev 1 (1957) 223, 32 (1988) 306

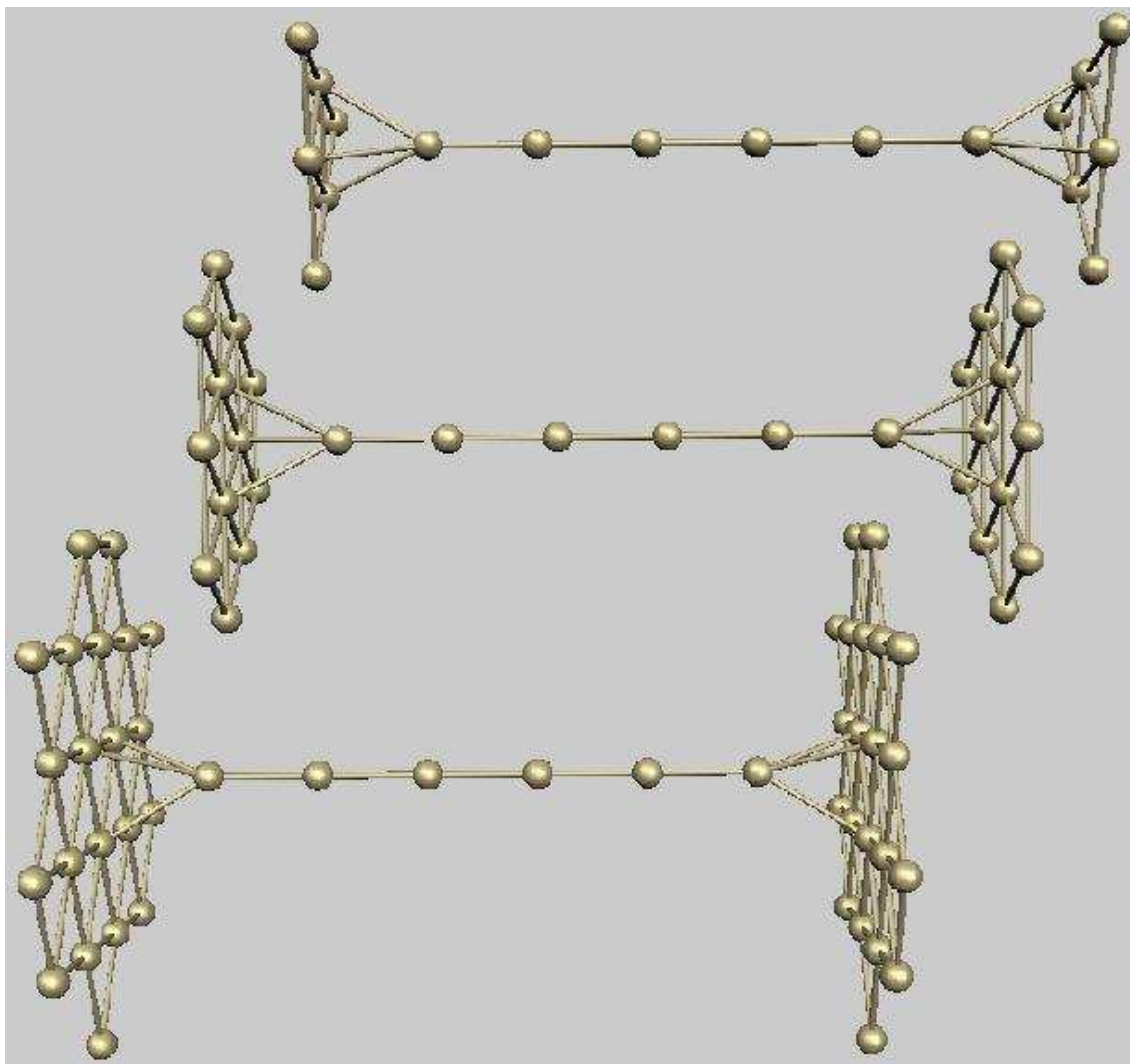


FIG. 1: (Color online) Extended quantum point contact (QPC) composed of a linear chain of six metal atoms. The chain plus clusters of size 6, 12, and 21 surface atoms defines the “extended molecule” for these systems.

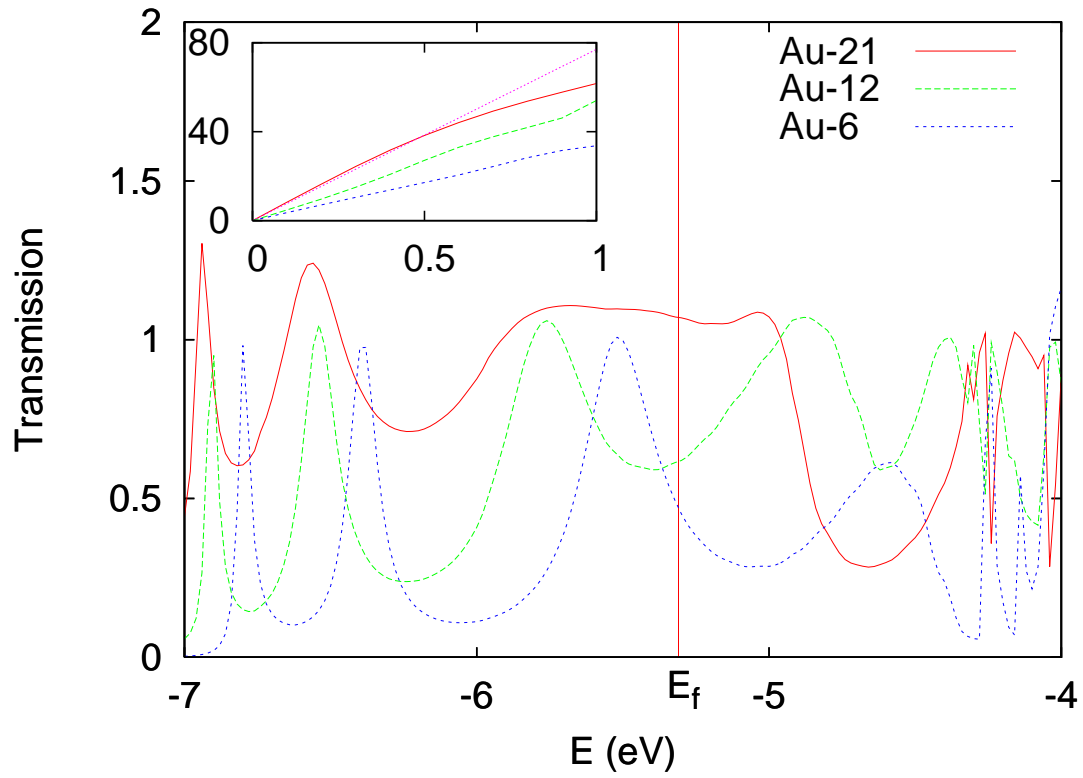


FIG. 2: (Color online) Transmission spectrum for linear Au chain with Au electrodes. Inset is corresponding IV curve where the upper dotted curve shows the theoretical maximum given by the quantum of conductance. Transmission increases with cluster size.

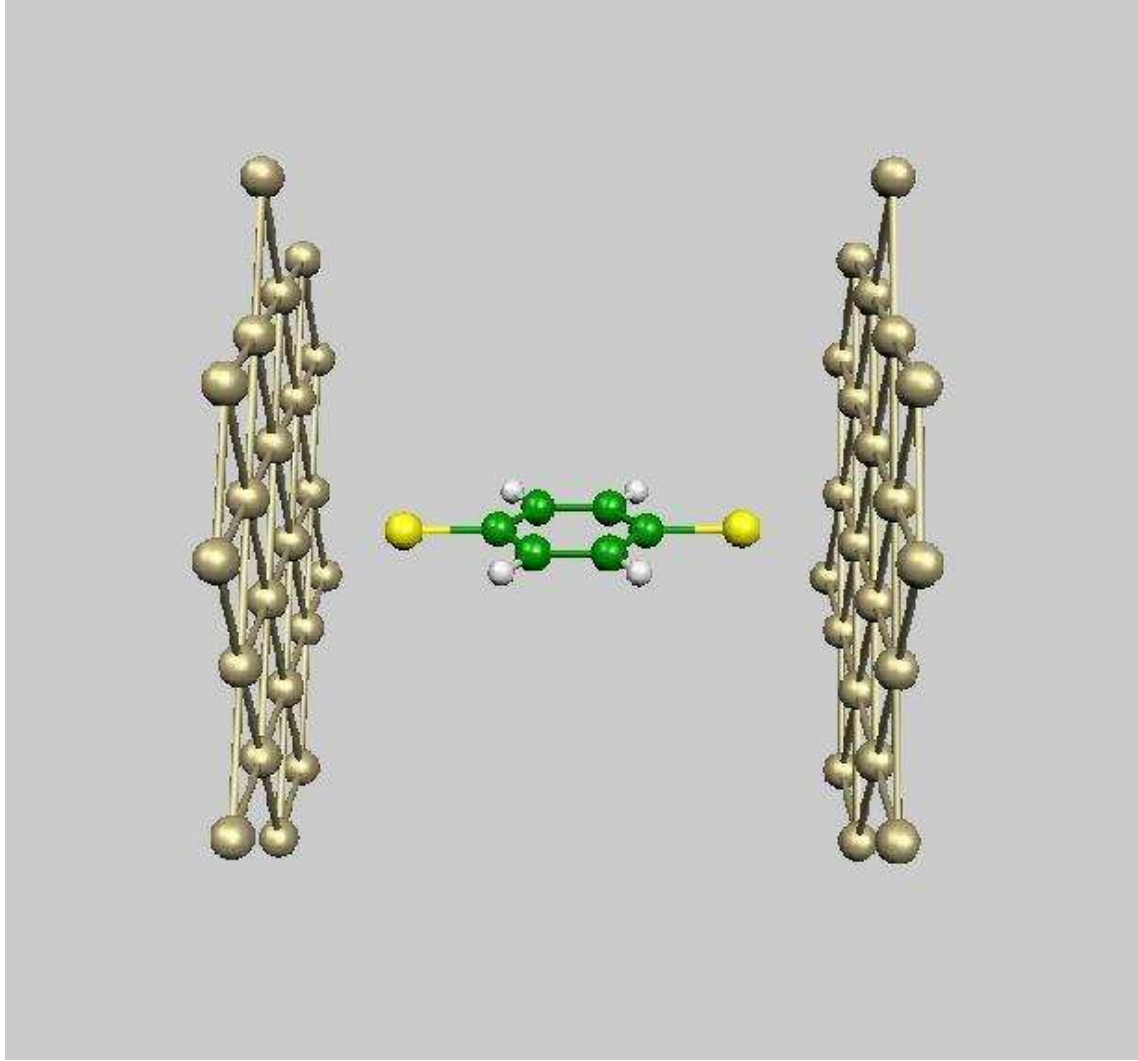


FIG. 3: (Color online) Extended molecule with phenyl dithiol (PDT) with clusters 21 metal surface atoms on each end. The extended molecule is coupled to an additional 63 atoms in the first and second layers and to the semi-infinite bulk through the self-energies.

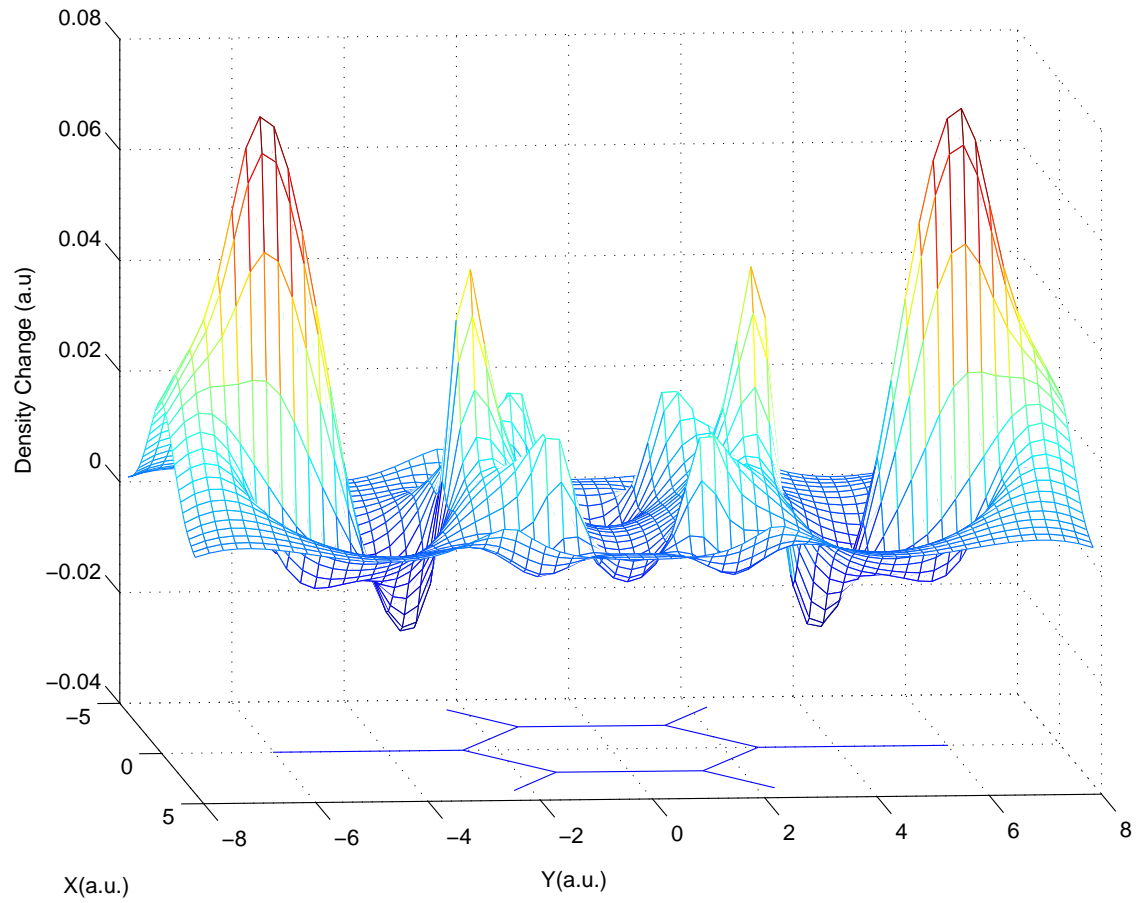


FIG. 4: (Color online) Spatial distribution of the charge density change upon formation of the contacts for Ag junction.

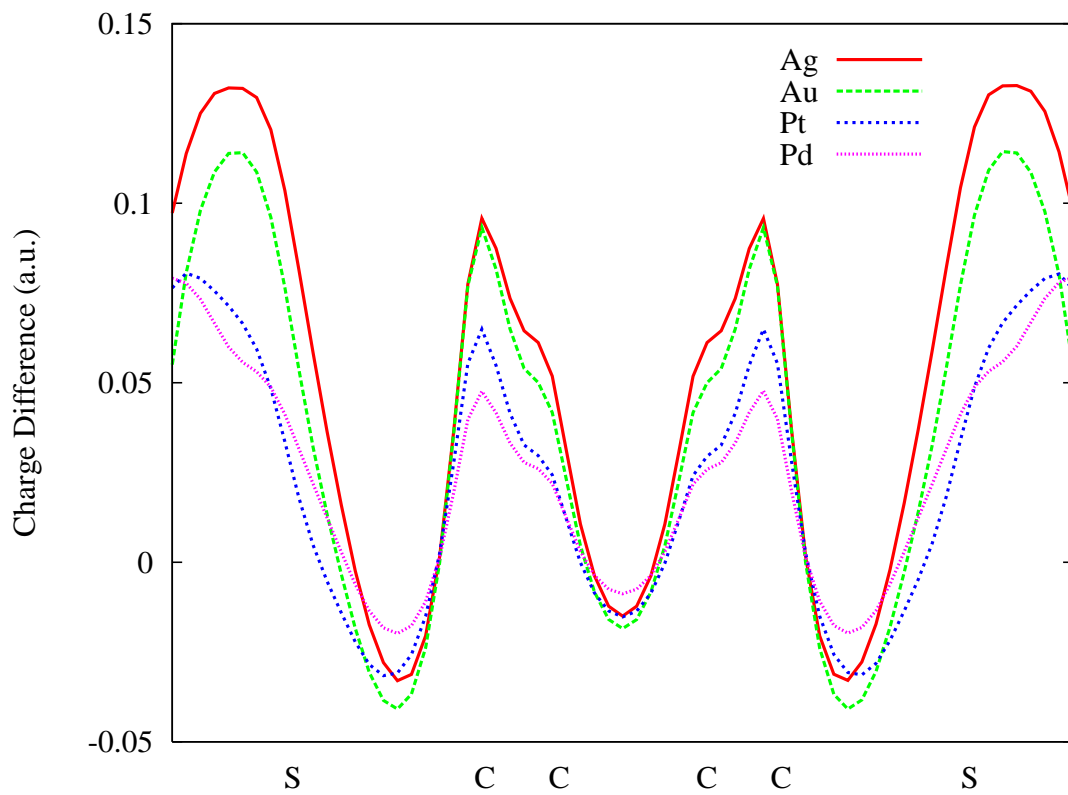


FIG. 5: (Color online) Comparison of the equilibrium charge density change along the axis of the molecule. The largest transfer is for Ag with Pd have the smallest.

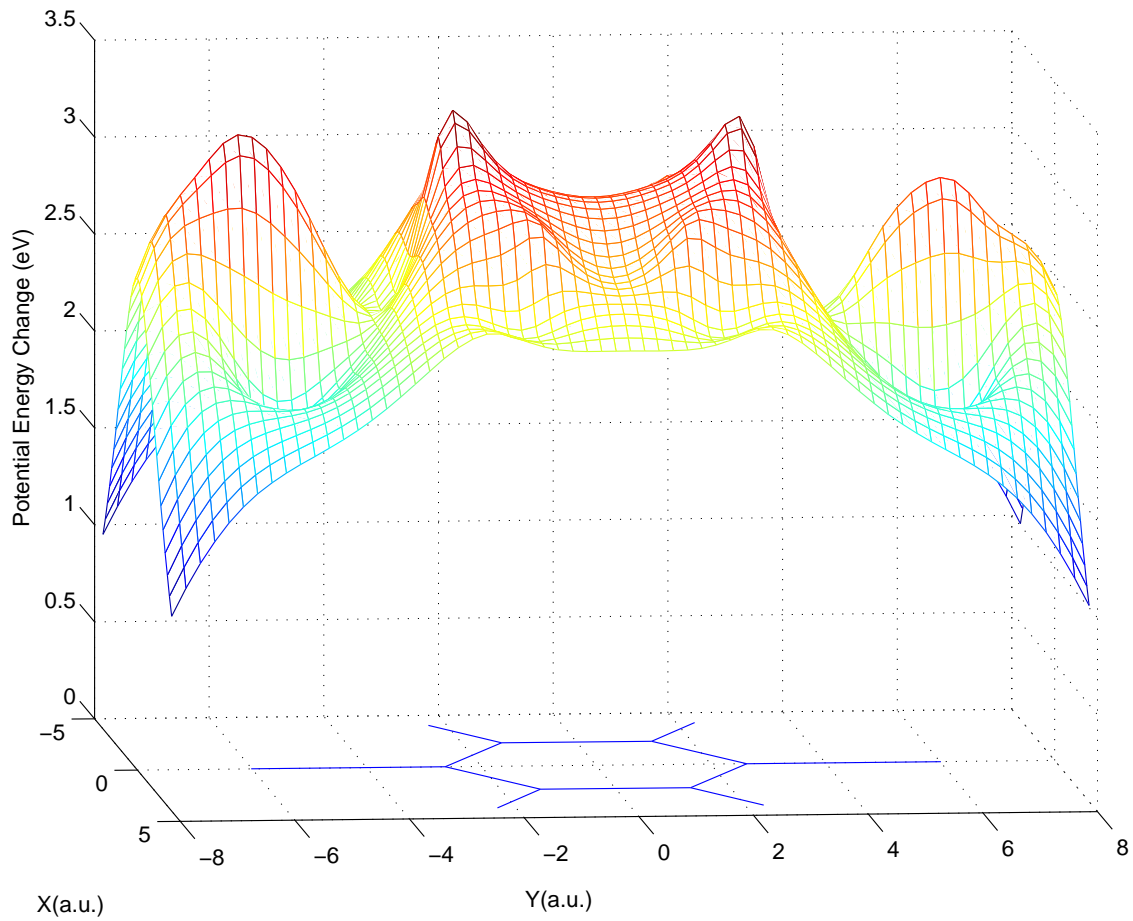


FIG. 6: (Color online) Spatial profile of the electrostatic potential energy change across the Ag junction. Potential barriers form near the sulfurs and adjacent carbons.

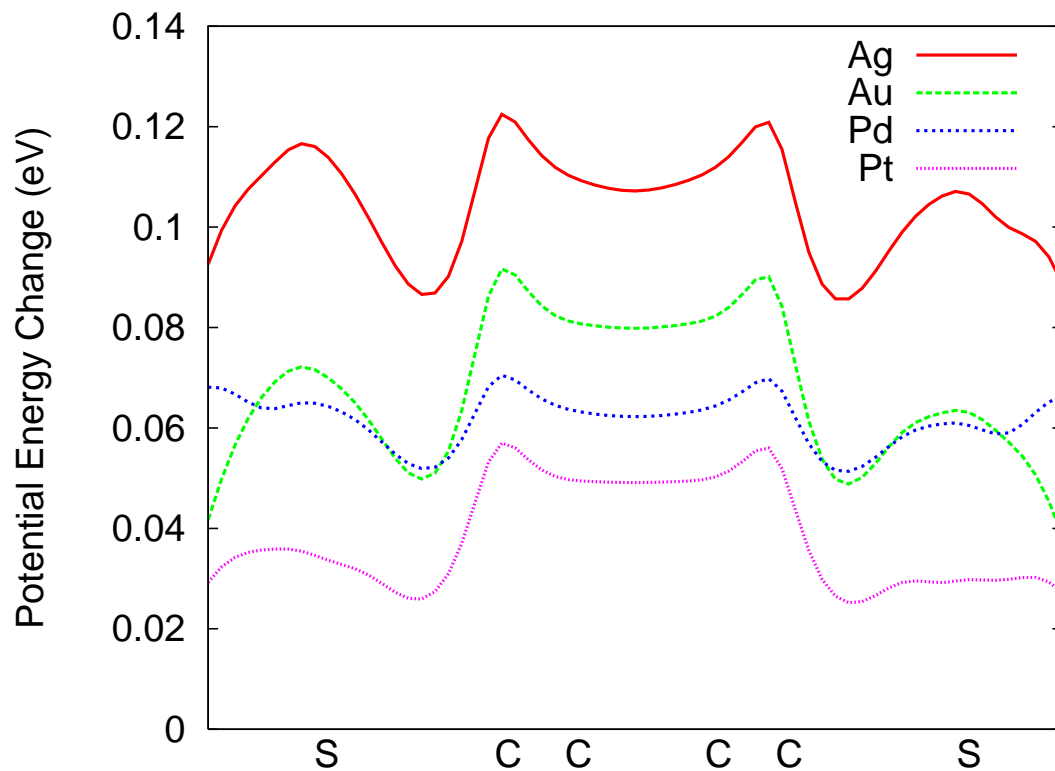


FIG. 7: (Color online) Comparison of the equilibrium electrostatic potential energy change along the axis of the molecule due to contact formation. The barrier for Ag is twice that of Au and four times that of Pt.

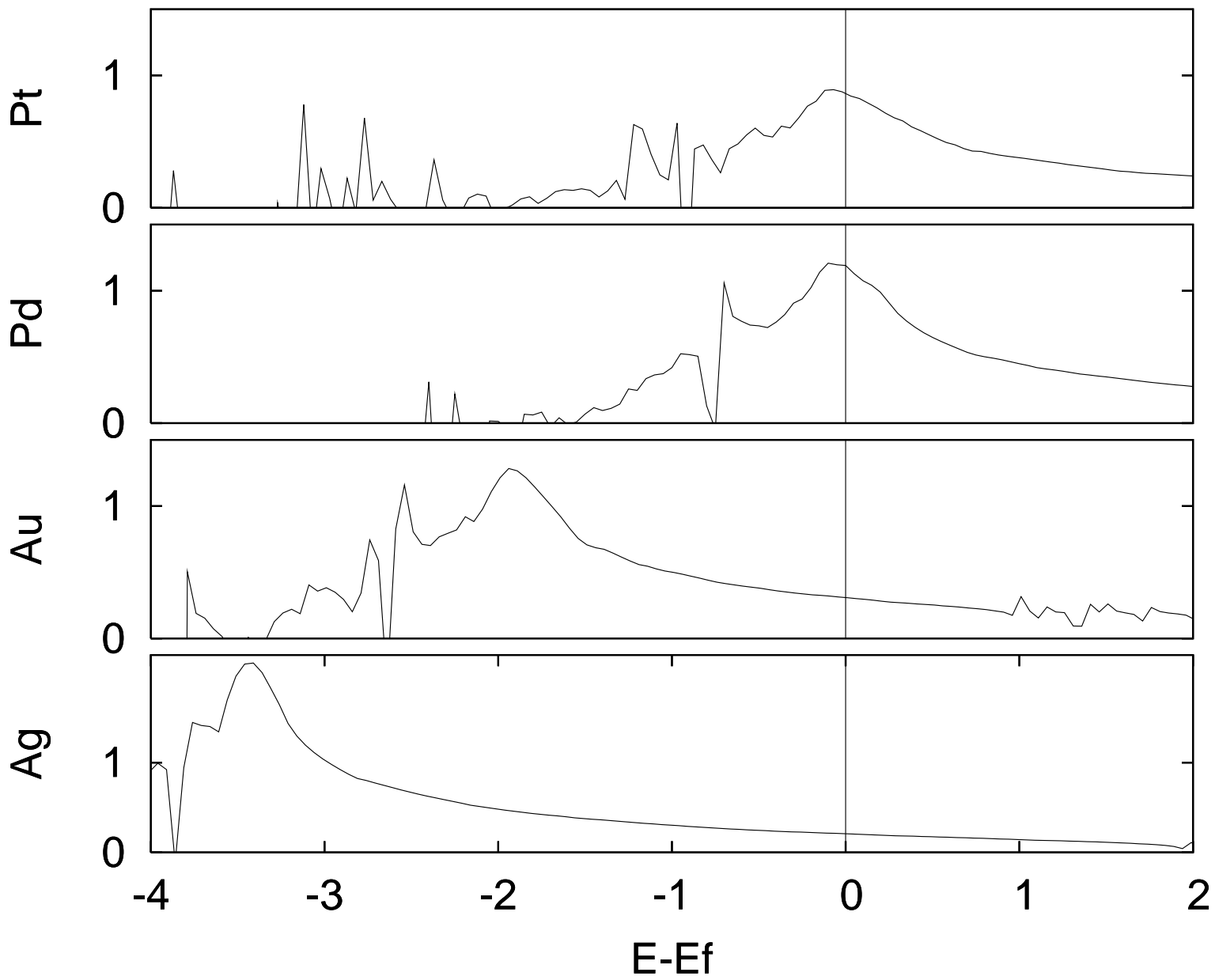


FIG. 8: DOS for the electrode metals calculated from the surface Green's function.

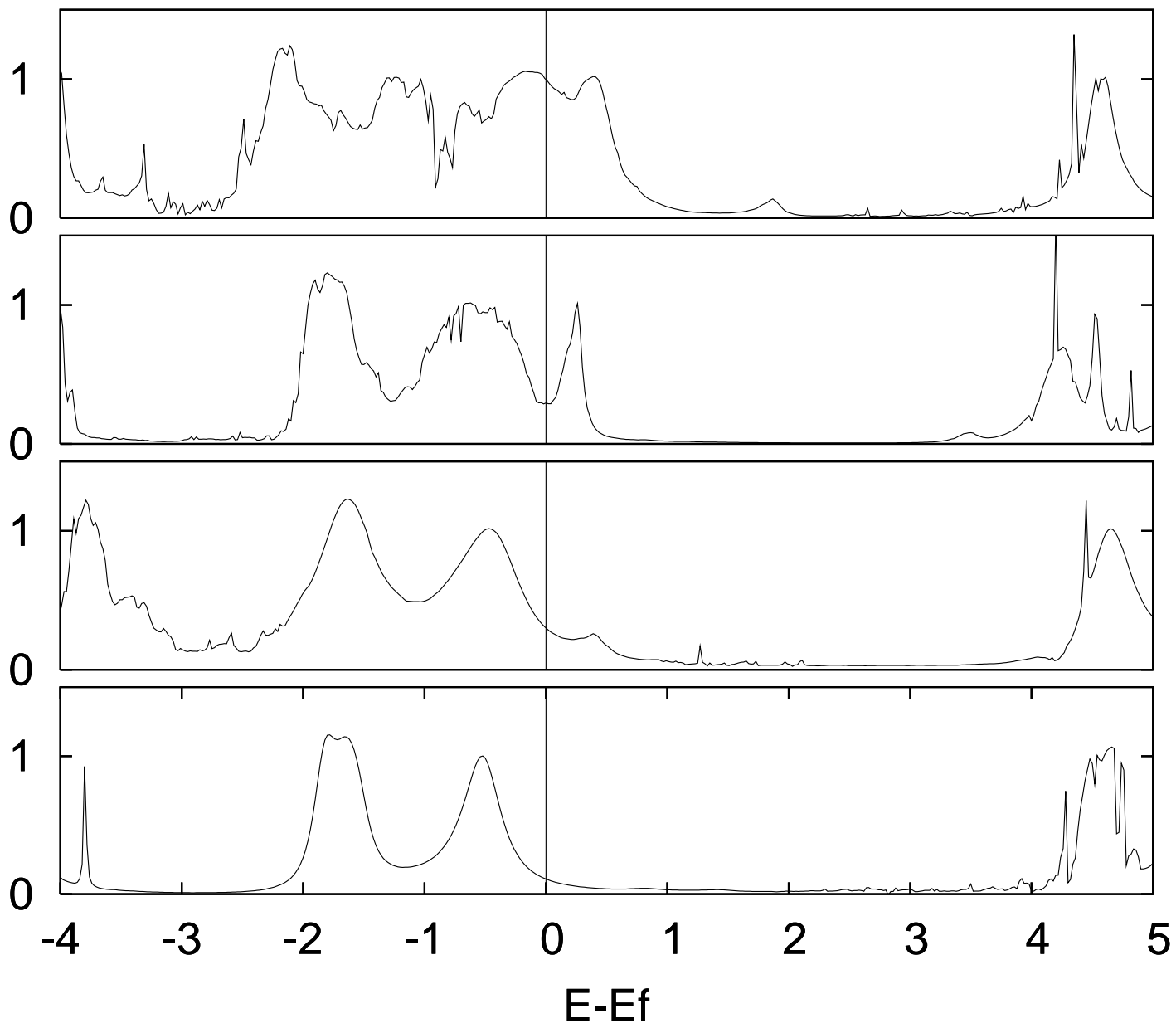


FIG. 9: Zero-bias transmission spectra for the four junctions.

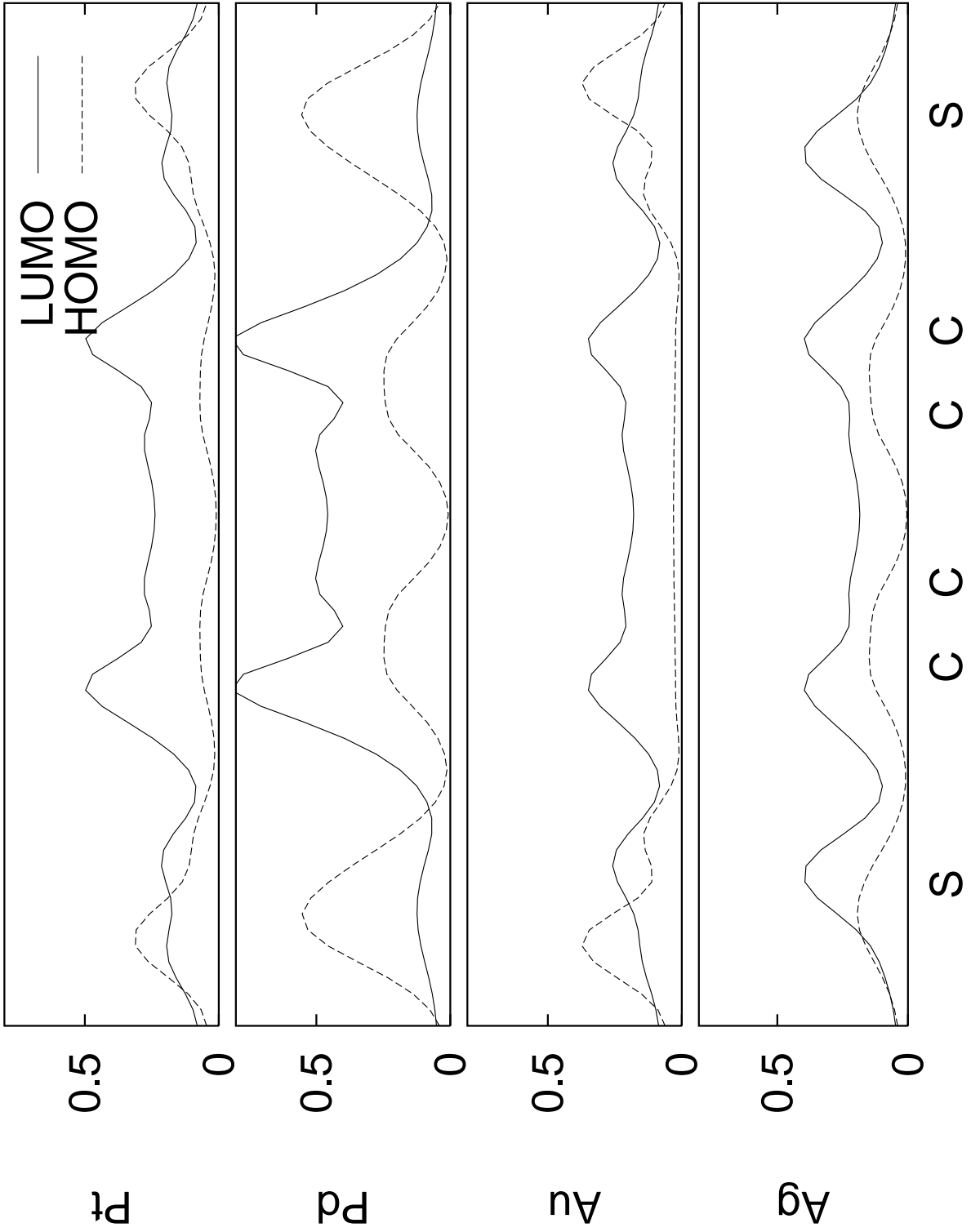


FIG. 10: Local DOS profile for the HOMO and LUMO for molecular junctions along the y-axis.

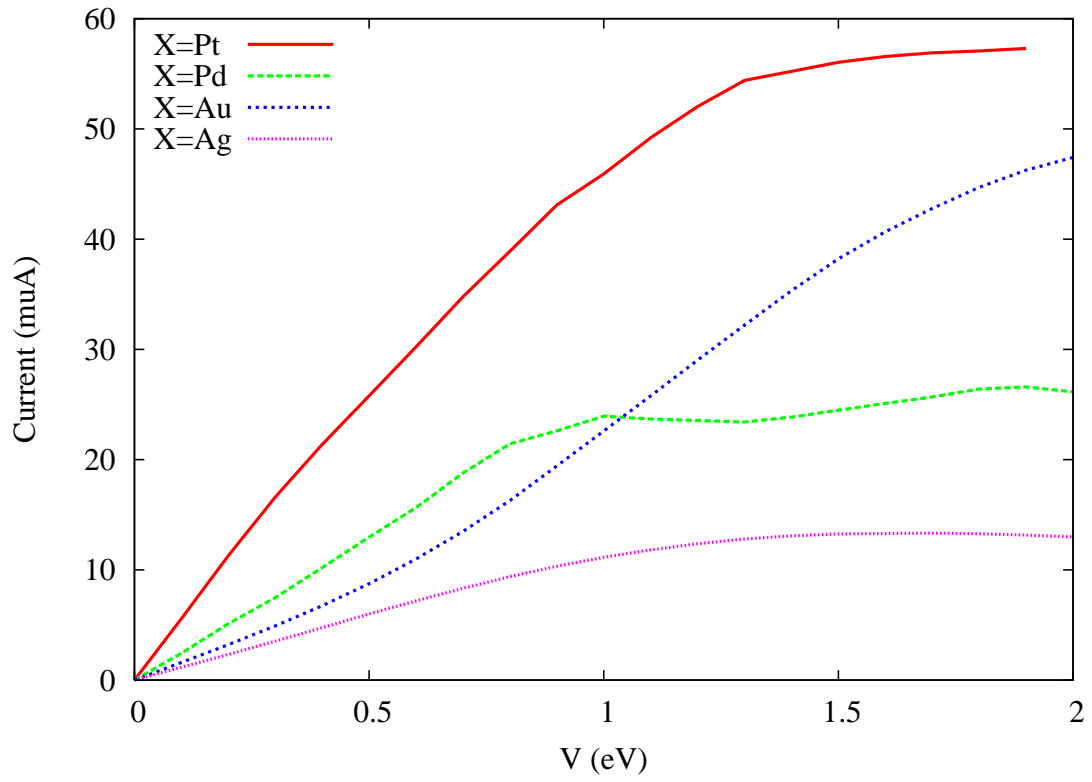


FIG. 11: (Color online) Comparison of IV characteristics as a function of metal.

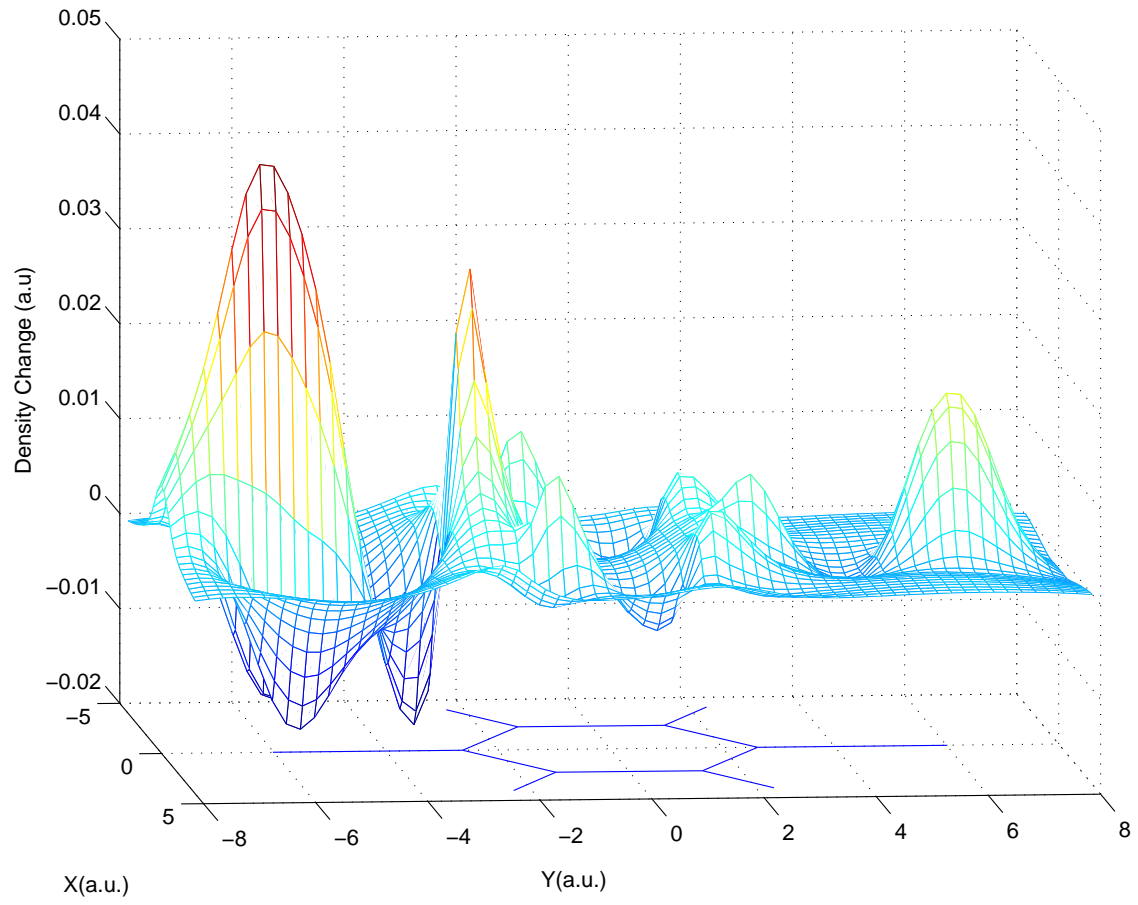


FIG. 12: (Color online) Spatial profile of charge density redistribution under bias of 1.8 V for Pd junction.

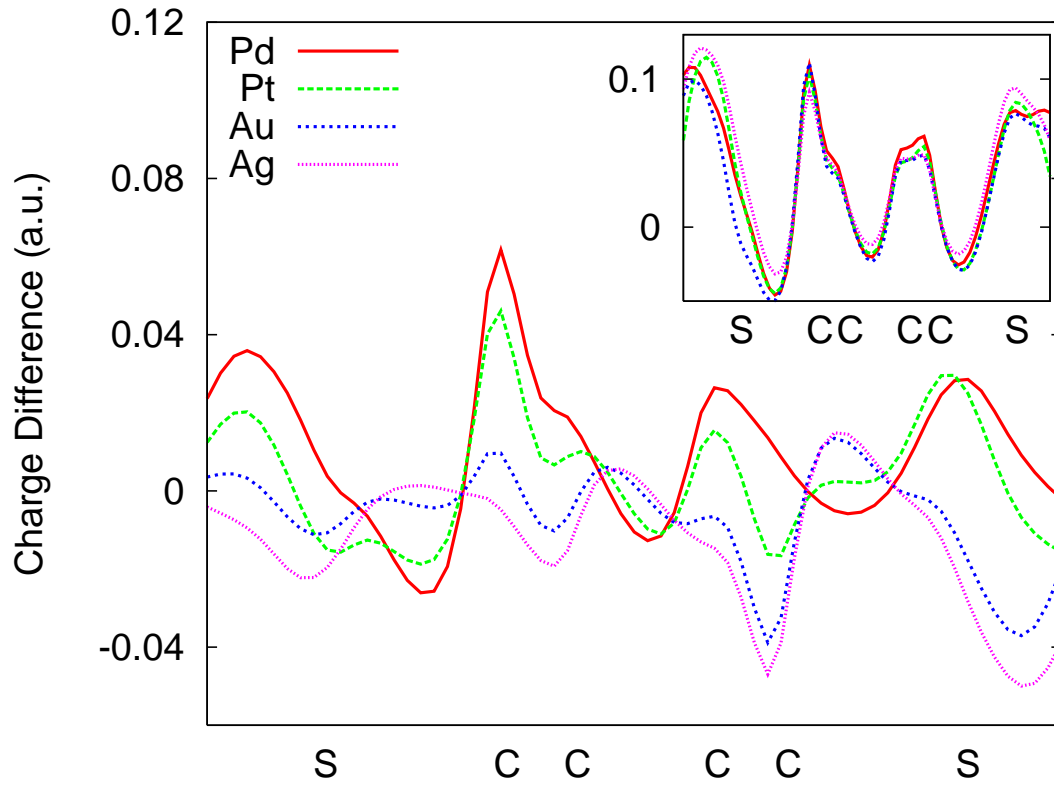


FIG. 13: (Color online) Comparison of charge density change under bias 1.8 V along the molecular axis for different junctions. Main plot is relative to equilibrium junction while inset is relative to isolated molecule and contacts.

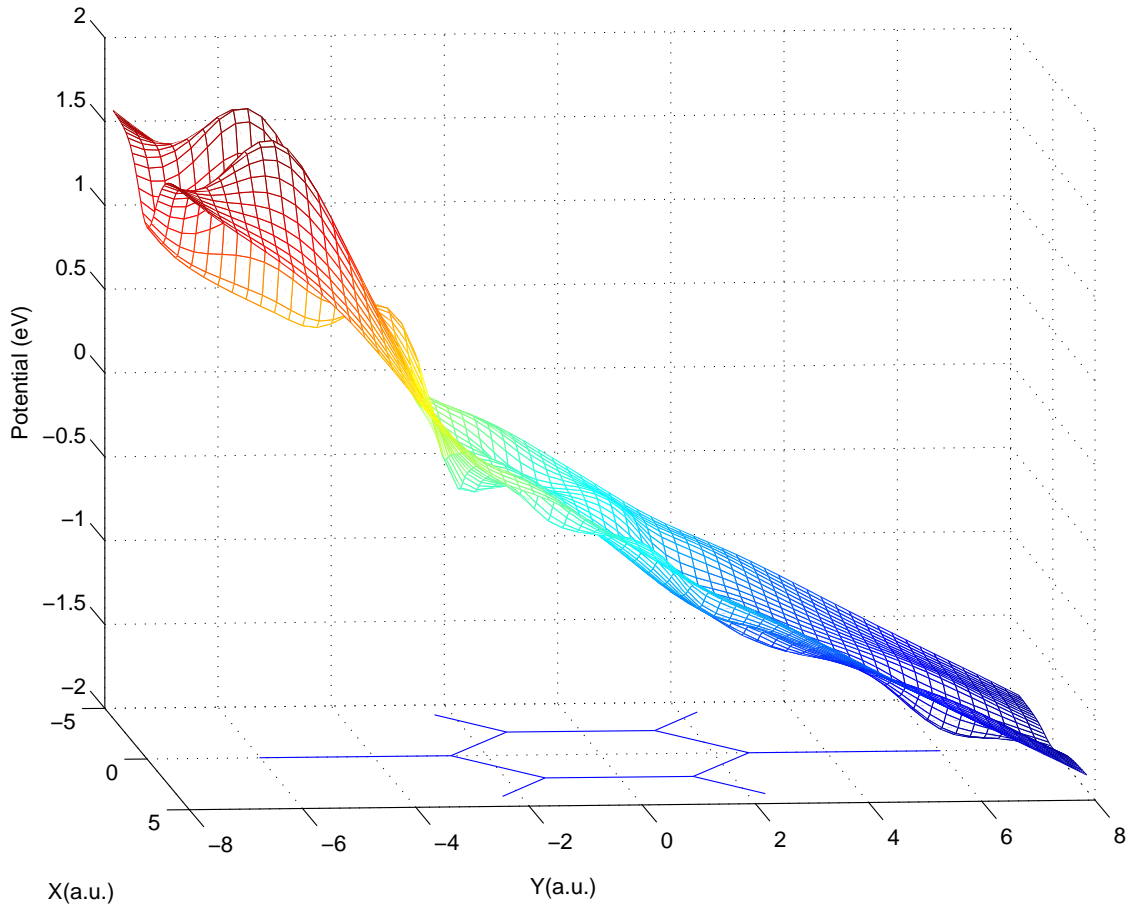


FIG. 14: (Color online) Spatial profile of electrostatic potential difference under bias of 1.8 V compared to equilibrium.

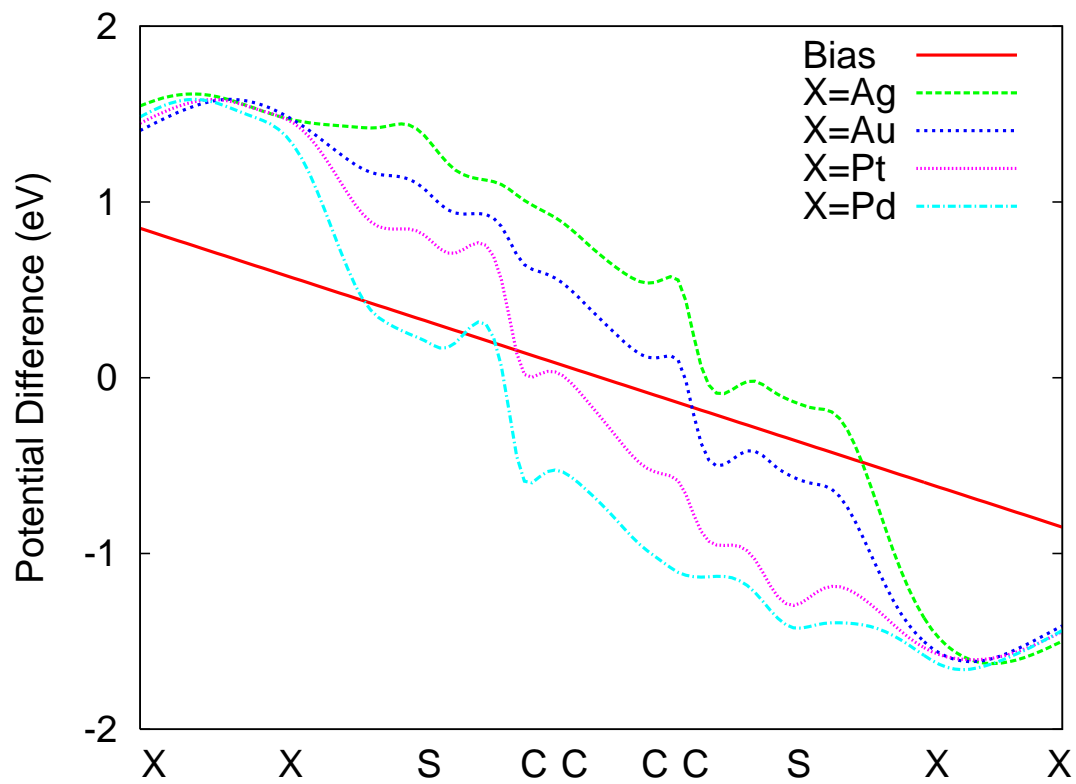


FIG. 15: (Color online) Comparison of potential differences under bias of 1.8 V along the molecular axis relative to equilibrium.